Journal of Nondestructive Evaluation (2022) 41:61
https://doi.org/10.1007/s10921-022-00892-z

# Delamination Defect Evaluation in CFRP Composite Patches by the Use of Active Thermography

**Amirreza Ardebili**[1] · **Mohammadreza Farahani**[1]

Received: 6 February 2022 / Accepted: 7 August 2022 / Published online: 5 September 2022


**Abstract**
Carbon fiber reinforced polymer composites (CFRPs) are widely used as repairing patches in the aerospace, automotive and oil and gas industries. Defects in the process of repairing with patches are in most cases inevitable. In this study, the effects of depth and dimension of separation defects on the intensity of thermal effect were investigated and evaluated by pulse thermography. Specimens made for testing were carbon fiber sheets that were patched onto the aluminum plate. In order to model the defects in different layers, edges, and center of the patch, interlayer separation was done by inserting kepton sheets between two samples with 4 and 8 layers of carbon laminates. The manufactured samples containing defects were then heated by the use of flash light and observed using the IR camera. The thermographic images and intensity plots were then compared for each sample. The results showed that there is a minor difference between results obtained by thermal images and plots for both defect size and the thermal intensity in the 4 layer patch sample. As for the 8 layer sample, the defect size differences % and the thermal intensity in the interfacial layer between Al-CFRP and sixth layer in the CFRP were higher. It was also found that the base metal has a significant influence on the identification of defects.

**Keywords** Composite repair patch · Non-destructive evaluation · Delamination defects · CFRP patch · Pulse thermography

## 1 Introduction

Non-destructive testing refers to inspection methods in which the performance of a part is analyzed without destroying it. Different Non-destructive techniques have their own advantages and disadvantages, such that some of the techniques are better than others for a particular application [1].

Infrared thermal thermography or imaging is a method for collecting, storing, and analyzing infrared radiant energy using infrared imaging systems. A thermal image is an image that shows the distribution of different levels of infrared radiant energy from a visible surface of the body. Infrared devices do not measure temperature and only measure radiant energy. Thermography is not an alternative to any other method of monitoring the condition, but it can be combined with other methods to produce positive and significant results [2]. This method can be divided into passive thermography and active thermography. Passive thermography measures the thermal changes of a material using an infrared camera device without external thermal stimulation sources [3]. In passive thermography, features of interest are abnormally inspected at higher or lower ambient temperatures. With passive thermography, it is possible to monitor the health status of composite structures, such as monitoring the rotor blade without stopping its operation. In addition, the mechanical damage and thermal behavior of the composite in mechanical tests can be obtained using active thermography [4, 5]. Unlike passive thermography, active thermography requires an external heat source to stimulate the test material. The main heat source can be a heat jet, hot water jet, hot air jet or a hot water bag. Optical heat sources are commonly used, such as high-power cinematographic lamps, infrared lines, high-power flash lamps, and laser beams. Many researches have been conducted in order to improve the capability of thermographic methods. In this regard, Garnier et al. [6] compared various NDT methods, including infrared thermography and ultrasonic testing and reported that if ultrasonic testing takes about 30 min, the infrared thermography inspection could be completed in 30 s. The use of the effusivity parameter in NDT was first discussed

✉ Mohammadreza Farahani
mrfarahani@ut.ac.ir

Amirreza Ardebili
amirreza.ardebili@ut.ac.ir

[1] School of Mechanical Engineering, College of Engineering, University of Tehran, 11155-4563 Tehran, Iran

by Balageas et al. [7]. The technique for determining diffusivity by applying flash heating was first suggested by Parker et al. [8]. A considerable issue in the infrared nondestructive evaluation is the identification of sound zone to detect the actual temperature contrast and the corresponding defect severity [9]. Sripragash et al. proposed a new segmentation technique for removing the non-uniformity effects in thermographic images. Ishikawa et al.[10] studied the inspection capability of active thermographic nondestructive inspection using laser scanning method. In their study, Carbon fiber reinforced plastic (CFRP) specimens were heated using a CO2 laser scanning device and their inspection capability was investigated. Their results showed that the temperature and phase behavior after laser scanning heating were similar to those after conventional instantaneous flash heating. They also observed that temperature contrast appearing on the defective surface varies depending on the scanning direction, such that it increases when the scanning direction is the same as the fiber direction of the laminates. Poelman et al. [11] performed a novel Adaptive Spectral Band Integration (ASBI) procedure for the postprocessing of flash thermographic datasets, which yields a unique damage index map. This procedure integrates the most useful spectral information for each pixel individually, obtaining a maximized defect detectability and an almost zero-reference level. ASBI was successfully applied on various composite coupons with flat bottom holes and barely visible impact damage, as well as on a stiffened aircraft composite panel with a complex cluster of production defects. In another study, Poelman et al. [12] introduced as a baseline-free image processing technique (an extension to the standard Gapped Smoothing Algorithm) called Multi-Scale Gapped Smoothing Algorithm (MSGSA). MSGSA uses the evaluation of a wide range of spatial gap sizes so that defects of highly different dimensions can be identified. It was also shown that a weighted combination of all assessed spatial gap sizes significantly improves the detectability of defects and results in an (almost) zero-reference background. Erazo-Aux et al. [13] presented a thermal imaging dataset for characterizing subsurface defective zones of CFRP(Carbon fiber reinforced polymer) and GFRP(Glass fiber reinforced polymer) material samples that were inspected by pulsed thermography. Palumbo et al. [14] quantitatively compared two algorithms based on the stepped thermography in order to optimize the testing time and signal to noise ratio. Hu et al. [15] proposed an infrared thermography technique and a long short-term memory recurrent neural network (LSTM-RNN) model that automatically classifies common defects occurring in honeycomb materials. This LSTM-based algorithm had 90% sensitivity in classifying water, and hydraulic oil ingress and 70% sensitivity in classifying debonding and adhesive pooling. Laureti et al. [16] used thermography and ultrasonic testing method to detect delamination in a glass/silicone composite. They showed that a frequency modulated chirp signal and pulse-compression can be used in active thermography for detecting delamination. Also, the same type of input signal and post-processing could be used to generate an image using air-coupled ultrasound. Alvarez-Restrepo et al. [17] worked on a method to evaluate defects in composite specimens based on image decomposition into a 2D orthogonal space. Their method was able to estimate the depths of defects up to 1.2 mm in CFRP and GFRP. In another study Alvarez-Restrepo et al. [18] developed a numerical model to estimate the thermal diffusivity through the anisotropic material that improves defect depth estimation between each layer. Vavilov et al. [19] studied the effect of impact on CFRP and GFRP sample using semi-automatic way with a small participation of the thermographer. This provided data spread from 0.6 to 2.4% for all evaluated parameters. The test results were statistically evaluated and revealed increasing values of effusivity/diffusivity as the impact energy increased and as second and third impacts were applied. Sreeshan et al. [20] developed a novel image segmentation method of thermal imaging using the computer vision algorithm and active contours in order to distinguish the de-bonds. Wen et al. [21] used a pulse-heating infrared thermography technique to detect and characterize bonding defects of CFRP patch on concrete structures. They used sequential thermal images to describe the temperature contrast and shapes of the bonding defects. Through analysis of the maximum temperature response, they investigated the effects of defect size and depth on the defect temperature response. The relationship between the defect depth and maximum temperature response was used to quantitatively estimate the defect depth. Sripragash and Sundaresan [22] presented an automated procedure for simultaneously eliminating spurious contrast and locating sound zone pixels, directly from experimental data in a thermographic NDT. Chung et al. [23] performed an experimental investigation on pulsed thermography to detect internal defects in industrial pipelines. Mac et al. [24] presented the quantification of delamination inside the concrete part of a specimen with a CFRP sheet installed on the surface via step heating thermography. The empirical thermal diffusivity of concrete girders strengthened with a CFRP sheet, is proposed in their study to predict delamination depths used for field investigations. Marani et al. [25] introduced a novel method for the automatic analysis of thermal signals resulting from the application of pulsed thermography. Input thermal decays were processed by a proper FIR filter designed to reduce the measurement noise, and then modeled to represent both sound regions and defective ones. Cruz-Aceves et al. [26] proposed a new image segmentation method based on multiple active contours guided by differential evolution, called MACDE. Pila et. al. [27] developed a method for calculating the thermal contrast by approximating the temperature profile of sound zone for a given surface called Differential

Absolute Contrast (DAC). Shepard et. al [28] developed the self-referencing thermographic method that eliminated the need for a representative sound zone. A similar method is also described by Omar [29]. In this approach, a set of surrounded pixels are selected where the temperature evolution of each pixel is compared with the average value of the total neighborhood pixels selected to find the defects. The effectiveness of this procedure highly depends on the location and size of the neighborhood pixels. Sinha et al. was characterized the delamination in PV modules by active infrared thermography [30]. They used a simulation approach to determine the optimum parameters for the delamination characterization. Different applications based on front and backsides of heating the module were also proposed in their paper. They proposed method had the potential to be employed for the quality check of PV modules during inline production. Ardebili et al. [31] previously tested the delamination defects in GFRP patches using step thermography. The reliability of a specific evaluation method depends on various factors, such as, the physical nature of the material under investigation, and the size and shape of the available specimen. GFRP and CFRP have differences in thermal properties such as thermal conductivity and thermal expansion that cause discrepancies in thermographic test results and defect identification. Consequently, we considered the nondestructive valuation of delamination defects in CFRP composite patches by the use of active thermography.

In the present study, the evaluation of defect depth, dimension, and location in the carbon fiber patches by the use of thermography has been conducted. One of the innovations of this research is the evaluation of different types of defects in terms of location (center and edge of patching), size and depth (patching layers) simultaneously.

## 2 Method

In this section, the manufacturing and preparation of samples as well as thermographic method used has been described.

### 2.1 Specimen Preparation

The patching operation is usually carried out in the aerospace industries where the most commonly used material used in these industries is aluminum 2024 [32]. This alloy has high functional operating and manufacturing capabilities in addition to strength for use in high tech industries. For this reason, the base material of the specimens chosen in this research is aluminum 2024-T4 with a thickness of 4 mm [33]. Carbon fiber is commonly used for repairing structures with composite patches. It is widely used in the manufacturing of aircraft, automobiles and military components due to its high strength and low weight [34]. Overall, two samples were made in this study consisting of 4 and 8 layers of carbon fiber having delamination defects as the repairing laminate for the Al plate. In order to model the defects, kepton sheets were inserted between the composite patch layers (Fig. 1).

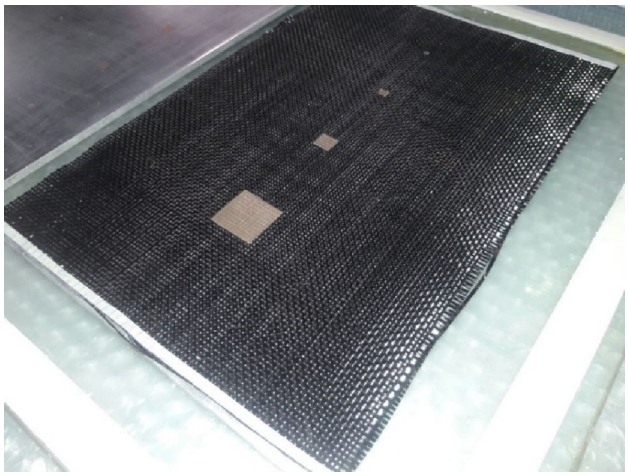

**Fig. 1** Defects placed on one of the layers

Base on the literature, there is a direct relationship between the size of the smallest detectable defect and the depth of the defect. The size of the smallest defect was considered 2.5 mm in this study. According to this defect size and preliminary experimental study, two composite samples with 4 and 8 layers were prepared for this study. The defects in the 4-layer patch sample were placed in the intersection between the patch and aluminum sheet (L0) and in the middle of the patch between the second and third layers (L2). In the case of the 8-layer patch sample, the defects were placed in the intersection between the patch and aluminum sheet (L0), between the second and third layers (L2), between the fourth and fifth layers (L4) and between the sixth and seventh layers (L6). Defect sizes were considered from the smallest to largest as 2.5 × 2.5 mm, 5 × 5 mm, 10 × 10 mm, and 25 × 25 mm in the center and 1 × 1,2.5 × 2.5, 5 × 5 and 12.5 × 12.5 in the edges of the sample. In order to avoid the interference of the thermal effects of the defects, they were arranged so that there was no intersection of the defects. The final size of the samples was 300 × 200 mm. The top view of the samples are shown in Figs. 2 and 3 for the 4 and 8 layer laminate samples, respectively. The depth of defects in this image was marked in each layer with a specific color. In addition, the layer number of the created defects was also shown using letter "L".

The vacuum infusion process (VIP) technique was used to make the samples[35]. The schematic of the patch fabrication process under the VIP and the VIP setup containing the actual samples are shown in Fig. 4. A template was used to place the abovementioned defects in their correct positions. The resin used in the CFRP was epoxy resin 2017 and the hardener was

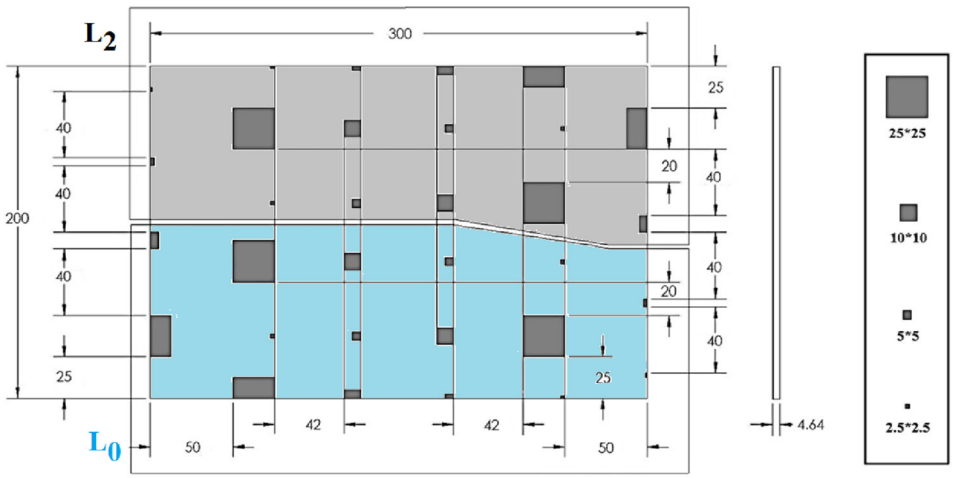


**Fig. 2** Patched 4-layer carbon fiber sample map

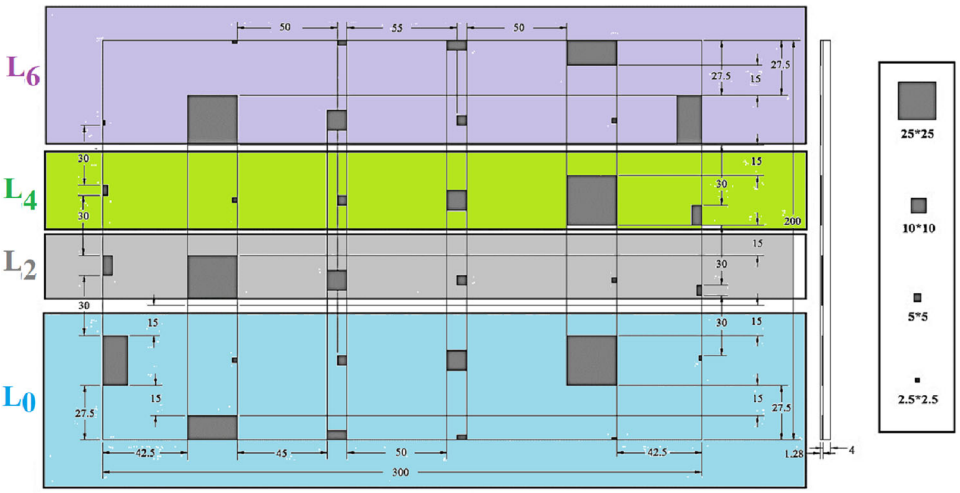


**Fig. 3** Patched 8-layer carbon fiber sample map

2018 EPOLAM with a ratio of 30/100 [36]. 200 g/m$^2$ plain carbon fabric from ACP composite ltd. was used to make the samples. The curing of the two samples was done at room temperature for three days.

For thermography testing, the surface must be optically opaque to minimize light reflection, eliminate noise in thermographic images, and maximize heat absorption. Therefore, the surface of the entire sample was sprayed with a thin layer of opaque black paint and dried by radiant heat in order to give a opaquer to the samples.

### 2.2 Thermographic Testing

In the active optical thermography method, optical heat sources such as a flash lamp or projector should be used to stimulate test specimens. The heat source used in this study is two tungsten lamp projectors with a power of 2 KW. The heat source distance was adjusted so as not to cause thermal concentration in a particular region of the sample and the thermal stimulation to be nearly uniform across the sample surface. The reflective arrangement was used such that the thermal excitation sources and the infrared camera were positioned on one side in front of the patched side of the sample. A modulator was used to generate the power required for the projectors as well as to supply DC pulse current. The board with four outputs along with four projectors were used. The camera used in the tests was Flir A325SC infrared camera with a resolution of $325 \times 240$ pixels with thermal sensitivity of 0.05 °C, a frequency of 60 Hz with a measuring accuracy of $\pm 2$ °C. The camera was placed such that only the sample being tested was in sight in order to prevent light reflection from the surroundings. Thermographic imaging was performed using Flir ResearchIR Mx + HSDR software.

## 3 Results and Discussion

Parameters investigated in process of defect identifications are depth, dimensions, and location of the defect. According to the experience gained in the fulfilled experiments,

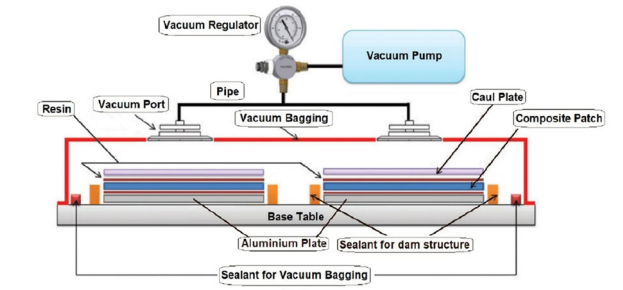


(a)

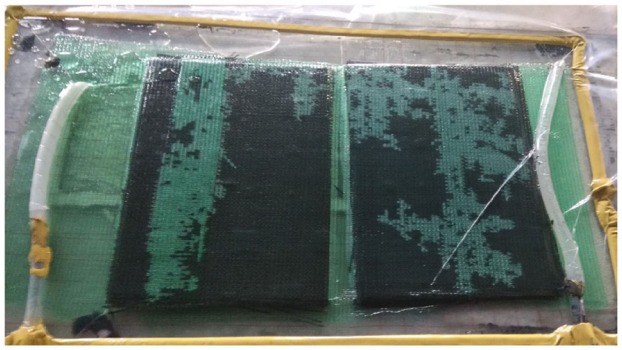

(b)

**Fig. 4** **a** Schematic of Double Vacuum Press technique, **b** curing of patch samples in the vacuum press

the timing of defects appearance is related to the power of the stimulation source. The timing parameters were selected based on a series of preliminary tests. The thermal excitation time of the samples and the considered cooling time of the samples were both 10 s. At best test condition, in the 4-layer patch sample with 10 s thermal stimulation time, defects with a difference of 20 °C relative to their surroundings were well detectable and in the 8-layer patch sample with 10 s thermal stimulation time, defects were well identifiable by a temperature difference of 10 °C relative to their surroundings. The best sharpness of the thermal images was obtained at the end of thermal stimulation phase and the first second of the cooling phase. Consequently, all the thermographic images used in the article are taken at the last second of stimulation. All results obtained from thermal images were without image processing.

### 3.1 Thermography Images

Based on the experimental results, it was found that the defect detection of the carbon fiber composite by pulse thermography was acceptable and the defects were detectable. A comparison between the thermographic images and the defect patterns of the 4 and 8 layers patch samples are shown in Figs. 5 and 6 respectably. As it is observed, in order to eliminate the ambient noise around the specimens, three images were taken for each sample. All defects except for the 2.5 × 2.5 mm ones were identified in both samples. The best sharpness was achieved for 25 × 25 mm defects which the edges are quite clear. Defects of 5 × 5 and 10 × 10 mm were also detectable, but lower sharpness was observed.

**Fig. 5** Thermal Images of the 4 layers patches

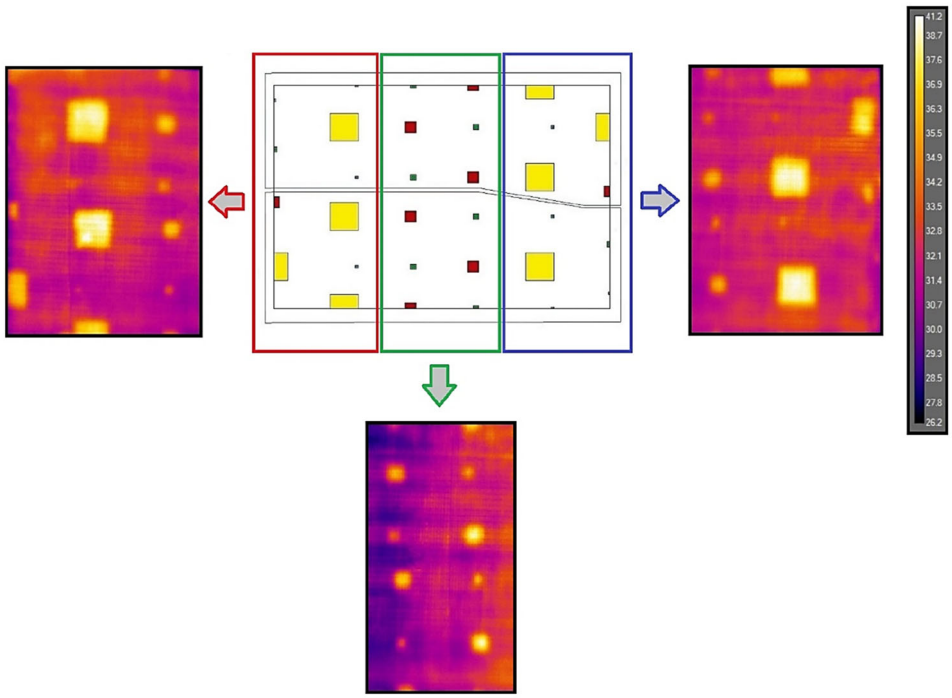

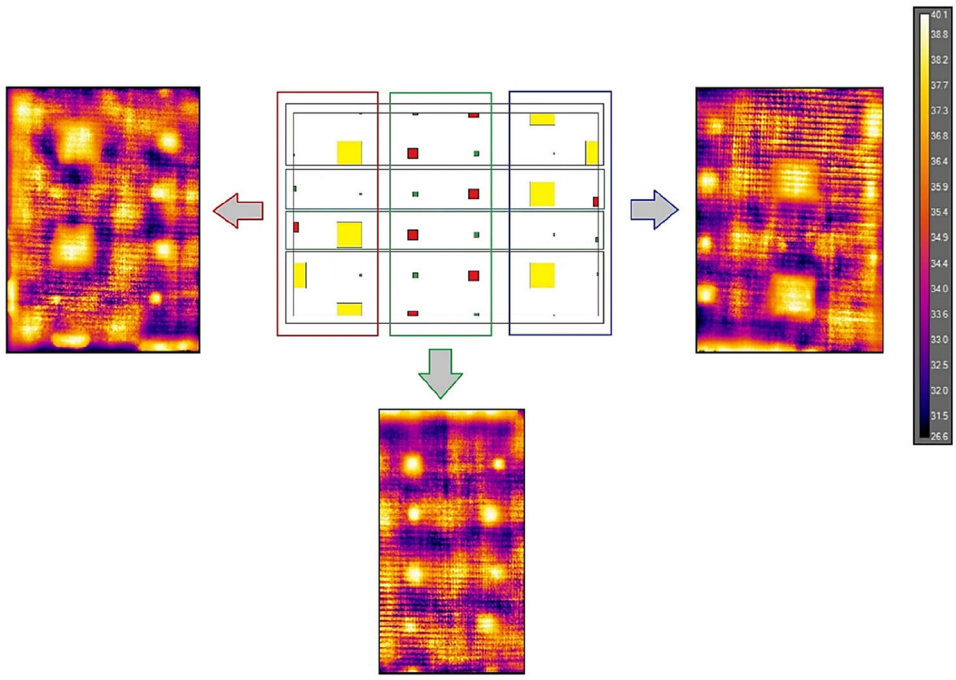

**Fig. 6** Thermal Images of the 8 layers patches

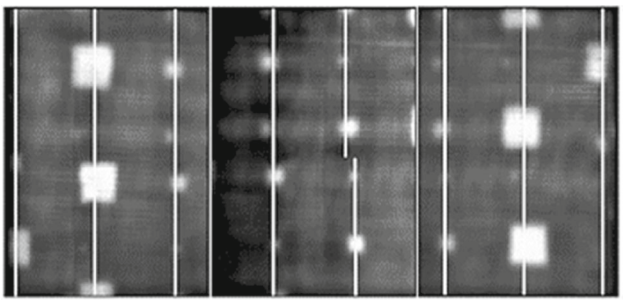

**Fig. 7** Examined paths for the evaluation of intensity and width of defects in center and edge of the 4-layer patch

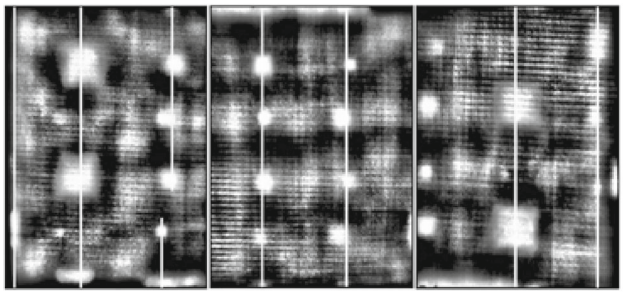

**Fig. 8** Examined paths for the evaluation of intensity and width of defects in center and edge of the 8-layer patch

## 3.2 Defect Dimension, Depth, and Location

In this section, the differences between the defect dimensions observed in the thermal images and the real defect dimensions were compared. In order to evaluate the defect size, a patch was defined through each defect which is observed in Figs. 7 and 8. Later, in order to quantify the effect of defect depth, a parameter called thermal intensity was defined [37]. This parameter expresses the difference between the temperature of the center of the defect and the temperature of the surrounding area of the defect. In the following, the effects of the defect depth on this parameter have been examined in detail.

The defect width was obtained by measuring and converting pixels to mm such that distance between the two points at the bottom of the thermal peak was defined as the defect width. Figures 7 and 8 illustrates the thermal intensity and defect width in the 4 and 8 layer samples. From the patch lines, data was extracted in the form of tables containing the thermal intensity and the size of the defects which were processed to interpret the defects.

### 3.2.1 Factors Affecting the Thermal Intensity

The investigations carried out in this article showed that the thermal effects of defects in the resulting thermal images are a function of the size and depth of the defect. In this article, the evaluation of the influences of these two parameters on the thermal intensity parameter, which defined in this article, was carried out. In this article, the quantitative effects of the size and depth of defects on the thermal intensity parameter have been discussed and interpreted in detail in various diagrams. Figures 9 and 10 show a comparison of the main factors affecting the thermal intensity of the identified defects. In these graphs, the effect of the depth and size of the defects on the thermal intensity of the detected

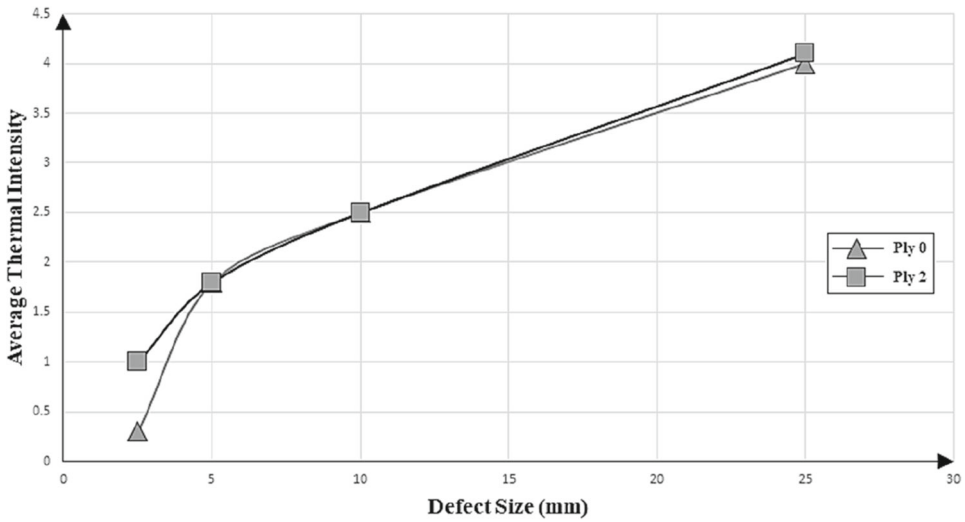


**Fig. 9** The effect of depth and size of defects on the thermal intensity of the defects identified in the 4-layer patch sample

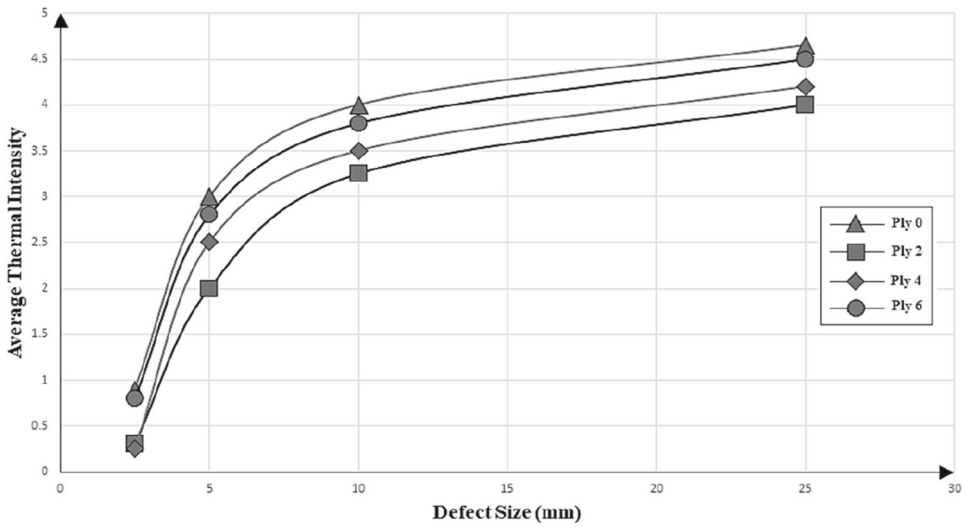


**Fig. 10** The effect of depth and size of defects on the thermal intensity of defects identified in the 8-layer patch sample

defects are compared. As it is observed, the larger the defect size, the higher the thermal intensity. The thermal intensity of the defects in each layer of the 4-layer sample is approximately constant which is due to the low thickness of the sample. In the 8 layer sample, the thermal intensity of the defects was highest in the 0 and 6 layer and lowest in layers 2nd and 4th. Thermal intensities were higher in the layers close to the heat source. The defect adjutancy to the aluminum plate also led to more thermal intensity. For both 4 and 8 layer patches, by increasing the defect size, the peak intensity was increased. It is clear that changes of thermal intensity parameter with the change of defect depth (for defects with the same size) have higher values for thicker samples.

A comparison was also conducted on the thermal intensity of the identified defects on the center and the edge of the patches. It was observed that the thermal intensity for the edge defects is slightly lower than the defects in the center of patches. As an overall outcome, the effect of the location of defects on thermal intensity is negligible, and so it is not mentioned in the graphs.

### 3.2.2 Factors Affecting the Defect Size

The most accurate measurement of embedded defects was seen for the central defect (25 mm × 25 mm). The least accurate measurement of embedded defect size was related to corner defects in the 8-layer patches with sizes of 1 × 2.5 mm and 2.5 × 5 mm. Figures 11, 12, 13, 14 illustrate the main influencing factors on the size difference (relative error %) between the detected defects and the real defect size. In the graphs, the effect of the depth and size on the relative error % is shown. As it could be seen, the relative error % decreases with increasing the defect depth. The mean relative error % of defects detected in the 4-layer sample was less than the mean difference % of defects detected in the 8-layer sample. As depicted in Figs. 11 and 12, the relative error % in the size of the defects in layer 2 was slightly lower than

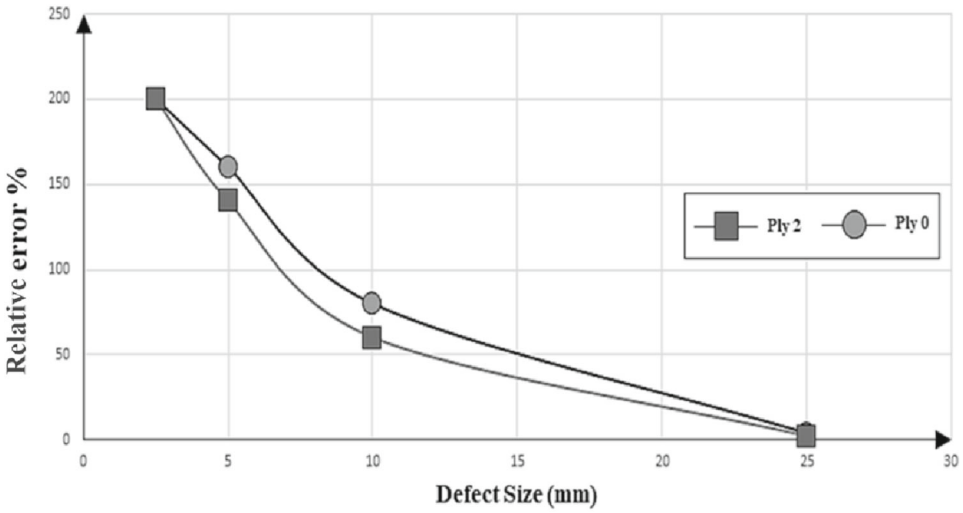


**Fig. 11** The effect of depth and size of defects on the relative error % of central defects detected in the 4-layer patch sample

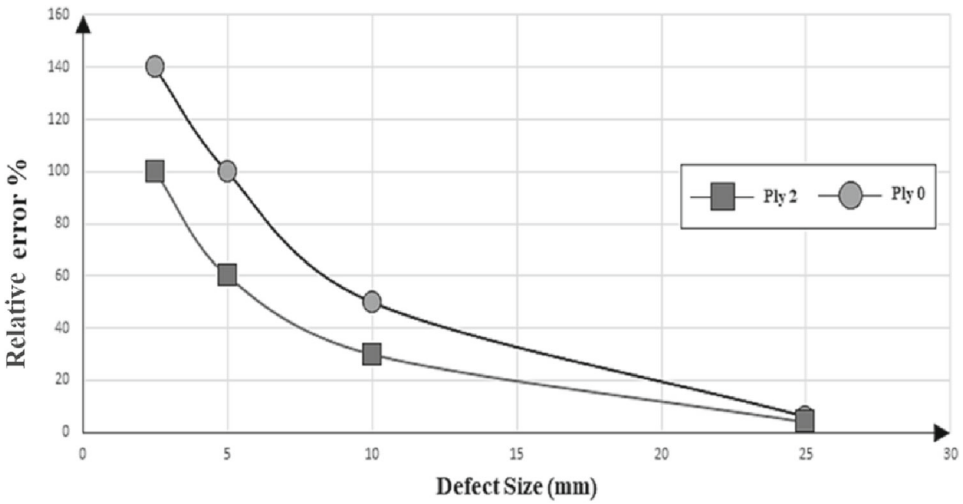


**Fig. 12** The effect of depth and size of defects on the relative error % of edge defects detected in the 4-layer patch sample

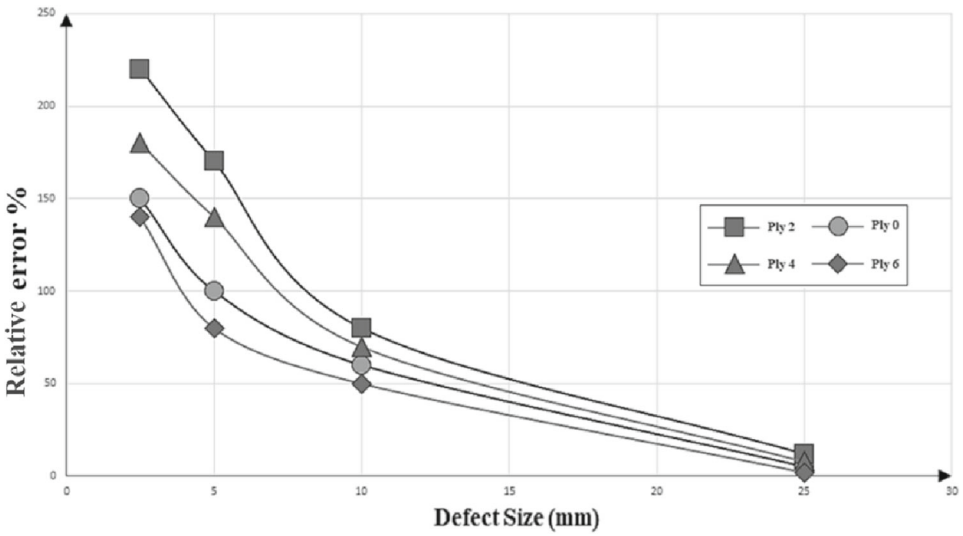


**Fig. 13** The effect of depth and size of defects on the relative error % of central defects detected in the 8-layer patch sample

in layer 0. The obtained result is consistent with the lower thermal intensity which is obtained for the defect in layer 0. Layer 2 was closer to the heat source that the thermal effects of these defects were more clear due to adjutancy to the heat source. In comparison between Figs. 11 and 12, it was shown that a similar trend exists for both central and

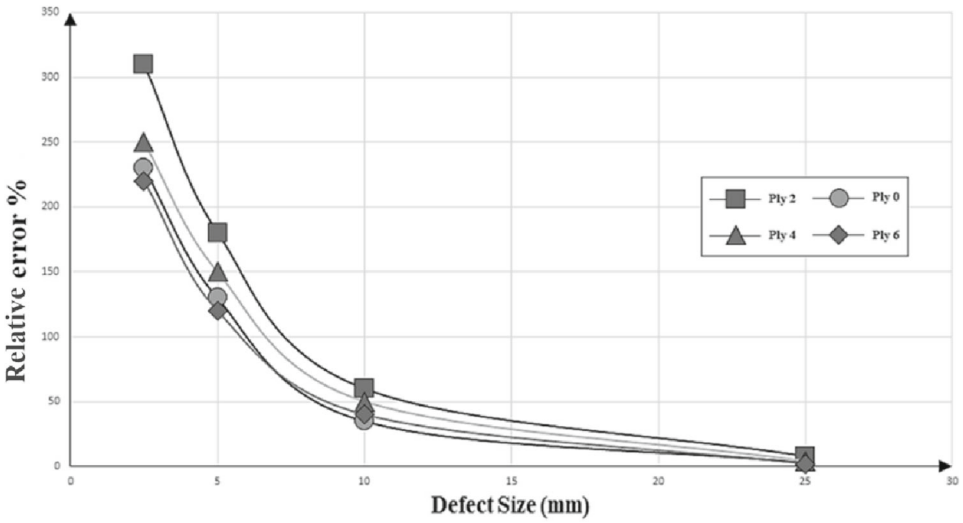


**Fig. 14** The effect of depth and size of defects on the relative error % of edge defects detected in the 8-layer patch sample

edge defects. Different heat transfer mechanisms for the edge defect led to a slightly more accurate defect size estimation. Also, generally, the low thickness of the 4-layers patch makes the measurement results of layers 0 and 2 closer together and makes it difficult to interpret. As illustrated in Figs. 13 and 14, the relative error % of the defects in layers 0 and 6 were higher than layer 2 and layer 4. It could be interpreted that the defects were more detectable. In Fig. 10, it was also shown that the defect closer to the heat source had a higher thermal intensity which led to more accurate size detection. On the contrary, the defect in the interface of the patch and base metal shown higher thermal intensity due to different heat conditions at the interface, which is consistent with lower relative error % observed in Figs. 13 and 14. As shown in Fig. 14, the size detection for the defects located at the edge of the patch is less accurate for some defects slightly which can be attributed to the different heat sink mechanisms for the edge defects. But in general, the central and edge defects present a similar trend in Figs. 13 and 14.

## 4 Conclusion

In thermography images, all the central defects except for the edge defects (2.5 × 2.5 mm defects) were identified in the 4 and 8 layer sample. This could be due to the convection of heat from the sample to the surrounding air in the defects adjacent to the edge of the samples. The thermal intensity of the defects close to the base metal and patch surface is higher than the defects located in other layers. The greater the size of the defects, the more thermal intensity emits itself. Due to the non-uniform heat transfer and different heat sink mechanisms, the thermal intensity of the central defects is a little more than edge defects. The mean of the defects thermal intensity in the 8 layer patch nearly equal to the 4 layer patch sample. In both 4 and 8 layer patches, the defect size detection close to the heat source, is more accurate. On the other hand, the defects at the interface of the patch and base metal plate are also detected accurately despite their high depth. The defect width estimation accuracy is proportional to the thermal intensity of the defects. In other words, higher the thermal intensity, lower the defect size difference %.

**Acknowledgements** All thermography tests were carried out at the Welding and Nondestructive Testing Applied Research Center of the University of Tehran (TWN) and hereby it is appreciated to provide the laboratory with the opportunity to conduct experiments and studies in this research.

**Authors' contributions** AA is the researcher who work under the supervision of MF.

**Funding** This research was conducted by personal support and there is no funding.

**Availability of data and material** There is no more data than what was presented in the article.

**Code availability (software application or custom code)** TNo code was used in this study.

## Declarations

**Conflicts of interest** Dr. Mohammadreza Farahani is the responsible author and there is no conflicts of interest in this research.

**Ethics approval**

Not applicable.

**Consent to participate**

Not applicable.

**Consent for publication**

Not applicable.

## References


1. Sabokrouh, M., Hashemi, S., Farahani, M.: Experimental study of the weld microstructure properties in assembling of natural gas transmission pipelines. Proc. Inst. Mech. Eng. Part B. **231**(6), 1039–1047 (2017). https://doi.org/10.1177/0954405415579581
2. Sam-Daliri, O., Farahani, M., Faller, L.-M., et al.: Structural health monitoring of defective single lap adhesive joints using graphene nanoplatelets. J. Manuf. Processes. **55**, 119–130 (2020). https://doi.org/10.1016/j.jmapro.2020.03.063
3. Meshkizadeh, P., Farahani, M.: Developing effective thermal signal processing to improve thermographic non-destructive inspection of metallic components. Nondestruct. Test. Eval. (2022). https://doi.org/10.1080/10589759.2021.2023521
4. Sam-Daliri, O., Faller, L.-M., Farahani, M., et al.: MWCNT–epoxy nanocomposite sensors for structural health monitoring. Electronics **7**(8), 143 (2018). https://doi.org/10.3390/electronics7080143
5. Sam-Daliri, O., Faller, L.-M., Farahani, M., et al.: Structural health monitoring of adhesive joints under pure mode I loading using the electrical impedance measurement. Eng Fract Mech. **245**, 107585 (2021). https://doi.org/10.1016/j.engfracmech.2021.107585
6. Garnier, C., Pastor, M.L., Eyma, F., Lorrain, B.: The detection of aeronautical defects in situ on composite structures using non destructive testing. Compos. Struct. **93**(5), 1328–1336 (2011). https://doi.org/10.1016/j.compstruct.2010.10.017
7. Balageas, P.C.D.L., Krapez, J.C.: Pulsed photothermal modeUng of layered materials. J. Appl. Phys. **59**(2), 348–357 (1986)
8. Parker, W.J., Jenkins, R.J., Butler, C.P., Abbott, G.L.: Flash method of determining thermal diffusivity, heat capacity, and thermal conductivity. J. Appl. Phys. **32**(9), 1679–1684 (1961). https://doi.org/10.1063/1.1728417
9. Sripragash, L., Sundaresan, M.: Non-uniformity correction and sound zone detection in pulse thermographic nondestructive evaluation. NDT & E Int. **87**, 60–67 (2017). https://doi.org/10.1016/j.ndteint.2017.01.006
10. Ishikawa, M., Ando, M., Koyama, M., Nishino, H.: Active thermographic inspection of carbon fiber reinforced plastic laminates using laser scanning heating. Compos. Struct. **209**, 515–522 (2019). https://doi.org/10.1016/j.compstruct.2018.10.113
11. Poelman, G., Hedayatrasa, S., Segers, J., Van Paepegem, W., Kersemans, M.: Adaptive spectral band integration in flash thermography: Enhanced defect detectability and quantification in composites. Compos. Part B Eng. (2020). https://doi.org/10.1016/j.compositesb.2020.108305
12. Poelman, G., Hedayatrasa, S., Segers, J., Van Paepegem, W., Kersemans, M.: Multi-scale gapped smoothing algorithm for robust baseline-free damage detection in optical infrared thermography. NDT E Int. (2020). https://doi.org/10.1016/j.ndteint.2020.102247
13. Erazo-Aux, J., Loaiza-Correa, H., Restrepo-Giron, A.D., Ibarra-Castanedo, C., Maldague, X.: Thermal imaging dataset from composite material academic samples inspected by pulsed thermography. Data Br. **32**, 106313 (2020). https://doi.org/10.1016/j.dib.2020.106313
14. Palumbo, D., Cavallo, P., Galietti, U.: An investigation of the stepped thermography technique for defects evaluation in GFRP materials. NDT E Int. **102**, 254–263 (2018). https://doi.org/10.1016/j.ndteint.2018.12.011
15. Hu, C., et al.: LSTM-RNN-based defect classification in honeycomb structures using infrared thermography. Infrared Phys. Technol. (2019). https://doi.org/10.1016/j.infrared.2019.103032
16. Laureti, S., et al.: Delamination detection in polymeric ablative materials using pulse-compression thermography and air-coupled ultrasound. Sensors (Switzerland) (2019). https://doi.org/10.3390/s19092198
17. Alvarez-Restrepo, C.A., Benitez-Restrepo, H.D., Tobón, L.E.: Characterization of defects of pulsed thermography inspections by orthogonal polynomial decomposition. NDT E Int. **91**, 9–21 (2017). https://doi.org/10.1016/j.ndteint.2017.05.003
18. Peeters, J., Ibarra-Castanedo, C., Sfarra, S., Maldague, X., Dirckx, J.J.J., Steenackers, G.: Robust quantitative depth estimation on CFRP samples using active thermography inspection and numerical simulation updating. NDT E Int. **87**, 119–123 (2017). https://doi.org/10.1016/j.ndteint.2017.02.003
19. Vavilov, V., Chulkov, A., Smotrov, A., Smotrova, S., Moskovchenko, A.: Characterizing impact damage in GFRP/CFRP composites by determining thermal effusivity/diffusivity. Meas. Sci. Technol. **30**(3), ab018e (2019). https://doi.org/10.1088/1361-6501/ab018e
20. Sreeshan, K., Dinesh, R., Renji, K.: Nondestructive inspection of aerospace composite laminate using thermal image processing. SN Appl. Sci. **2**(11), 1–14 (2020). https://doi.org/10.1007/s42452-020-03619-9
21. Wen, B., et al.: Pulse-heating infrared thermography inspection of bonding defects on carbon fiber reinforced polymer composites. Sci. Prog. **103**(3), 1–14 (2020). https://doi.org/10.1177/0036850420950131
22. Sripragash, L., Sundaresan, M.: Non-uniformity correction and sound zone detection in pulse thermographic nondestructive evaluation. NDT E Int. **87**, 60–67 (2017). https://doi.org/10.1016/j.ndteint.2017.01.006
23. Chung, Y., Shrestha, R., Lee, S., Kim, W.: Thermographic inspection of internal defects in steel structures: analysis of signal processing techniques in pulsed thermography. Sensors (Switzerland) **20**(21), 1–17 (2020). https://doi.org/10.3390/s20216015
24. Mac, V.H., Huh, J., Doan, N.S., Shin, G., Lee, B.Y.: Thermography-based deterioration detection in concrete bridge girders strengthened with carbon fiber-reinforced polymer. Sensors (Switzerland) **20**(11), 1–19 (2020). https://doi.org/10.3390/s20113263
25. Marani, R., Palumbo, D., Galietti, U., Stella, E., D'Orazio, T.: Enhancing defects characterization in pulsed thermography by noise reduction. NDT E Int. **102**, 226–233 (2018). https://doi.org/10.1016/j.ndteint.2018.12.009
26. Cruz-Aceves, I., et al.: Multiple active contours guided by differential evolution for medical image segmentation. Comput. Math. Methods Med. (2013). https://doi.org/10.1155/2013/190304
27. Pilla, M., Klein, M., Maldague, X., Salerno, A.: New absolute contrast for pulsed thermography. InProc. QIRT **1**(1), 53–58 (2002). https://doi.org/10.21611/qirt.2002.004
28. Shepard, S.M., Rubadeux, B.A., Ahmed, T.: Automated thermographic defect recognition and measurement. AIP Confer. Proc. **373**, 373–378 (2008). https://doi.org/10.1063/1.1302030
29. Omar, M., Hassan, M.I., Saito, K., Alloo, R.R.: IR self-referencing thermography for detection of in-depth defects Department of Mechanical Engineering, University of Kentucky Lexington KY 40506-0503 Toyota Motor Manufacturing North America Inc., pp. 1–17
30. Sinha, A., Sastry, O.S., Gupta, R.: Detection and characterisation of delamination in PV modules by active infrared thermography. NDT & E Int. **31**(1), 1–16 (2016). https://doi.org/10.1080/10589759.2015.1034717
31. Ardebili, A., Hossein, M.A.: Non-destructive testing of delamination defects in GFRP patches using step heating thermography. NDT & E Int. (2022). https://doi.org/10.1016/j.ndteint.2022.102617
32. Ghabezi, P., Farahani, M., Shahmirzaloo, A., et al.: Defect evaluation of the honeycomb structures formed during the drilling

process. Int J Damage Mech. **29**(3), 454–466 (2020). https://doi.org/10.1177/1056789519860573
33. Farhang, M., Farahani, M., Enami, M.: Experimental study on the effects of friction stir spot welding process parameters on AL2024T3 joint strength. ADMT J. **14**(4), 105–112 (2021). https://doi.org/10.30495/ADMT.2021.1922979.1280
34. Ghabezi, P., Farahani, M.: A cohesive model with a multi-stage softening behavior to predict fracture in nano composite joints. Eng. Frac. Mech. **219**, 106611 (2019). https://doi.org/10.1016/j.engfracmech.2019.106611
35. Ghabezi, P., Farahani, M.: Experimental investigation of nanoparticles effects on cohesive model and bridging laws of mode I fracture in the adhesive joints. J. Adhes. Sci. Technol. **31**(16), 1807–1823 (2017). https://doi.org/10.1080/01694243.2017.1284639
36. Ghabezi, P., Farahani, M.: Characterization of cohesive model and bridging laws in mode I and II fracture in nano composite laminates. J. Mech. Eng. Sci. **12**(4), 4329–4355 (2018). https://doi.org/10.15282/jmes.12.4.2018.24.0370
37. Howell, J.R., Mengüç, M.P., Daun, K., Siegel, R.: Thermal radiation heat transfer. CRC Press, New York (2020)